

This item is likely protected under Title 17 of the U.S. Copyright Law. Unless on a Creative Commons license, for uses protected by Copyright Law, contact the copyright holder or the author.

Access to this work was provided by the University of Maryland, Baltimore County (UMBC) ScholarWorks@UMBC digital repository on the Maryland Shared Open Access (MD-SOAR) platform.

Please provide feedback

Please support the ScholarWorks@UMBC repository by emailing scholarworks-group@umbc.edu and telling us what having access to this work means to you and why it's important to you. Thank you.



TRANSPORT OF SOLAR WIND H^+ AND He^{++} IONS ACROSS EARTH'S BOW SHOCK

G. K. PARKS¹, E. LEE², S. Y. FU³, H. E. KIM⁴, Y. Q. MA³, Z. W. YANG⁵, Y. LIU⁵, N. LIN¹, J. HONG⁴,
P. CANU⁶, I. DANDOURAS⁷, H. RÈME⁷, AND M. L. GOLDSTEIN⁸

¹ Space Sciences Laboratory, University of California, Berkeley, CA, USA; parks@ssl.berkeley.edu

² School of Space Research and Institute of Natural Sciences, Kyung Hee University, Yongin, Korea

³ Institute of Space Science, Peking University, Beijing, China

⁴ School of Space Research, Kyung Hee University, Yongin, Korea

⁵ Key Laboratory for Space Weather, Chinese Academy of Sciences, Beijing, China

⁶ Plasma Physics Laboratory, Ecole Polytechnique, Paris, France

⁷ IRAP, Paul Sabatier University and CNRS, Toulouse, France

⁸ NASA Goddard Space Flight Center, Greenbelt, MD, USA

Received 2016 May 25; accepted 2016 June 7; published 2016 July 8

ABSTRACT

We have investigated the dependence of mass, energy, and charge of solar wind (SW) transport across Earth's bow shock. An examination of 111 crossings during quiet SW in both quasi-perpendicular and quasi-parallel shock regions shows that 64 crossings had various degrees of heating and thermalization of SW. We found 22 crossings where the SW speed was $<400 \text{ km s}^{-1}$. The shock potential of a typical supercritical quasi-perpendicular shock estimated from deceleration of the SW and cutoff energy of electron flat top distribution is ~ 50 Volts. We find that the temperatures of H^+ and He^{++} beams that penetrate the shock can sometimes be nearly the same in the upstream and downstream regions, indicating little or no heating had occurred crossing the bow shock. None of the models predict that the SW can cross the bow shock without heating. Our observations are important constraints for new models of collisionless shocks.

Key words: shock waves – solar wind

1. INTRODUCTION

The problem of understanding collisionless shocks has been at the forefront of experimental and theoretical space plasma physics research for many decades. Although much is known about collisionless shocks, the mechanisms of heating and thermalization still remain poorly understood. Shocks are *irreversible* and the shock boundary represents a transition between two regions of local thermodynamic equilibrium (Krall 1997). Standard shock theories predict that the solar wind (SW) flow dissipates while crossing the bow shock and becomes subsonic, and the downstream region is populated with thermalized SW (Kennel et al. 1985). The SW is collisionless, however, and how thermalization could occur without collisions has been the interest of many theoretical studies (Auer et al. 1971; Wu et al. 1984; Kennel et al. 1985; Gedalin 1997; Krall 1997; Ellacot & Wilkinson 2003; Chapman et al. 2005).

Observations since the early space era, however, have indicated that many features of the SW interaction with Earth's bow shock are different from the predictions of shock theories. For example, *HEOS-1* (Formisano et al. 1970) has shown that while thermalization of H^+ generally occurs across the shock boundary, sometimes the SW He^{++} ions are found with unchanged energy spectra downstream of the shock, in the magnetosheath (MS). The ISEE mass spectrometer results showed that both SW H^+ and He^{++} beams could be found in the MS with the same bulk velocities (Peterson et al. 1979). Furthermore, AMPTE observations reported that He^{++} and O^{+6} ions in the MS had shell-like distributions (Fuselier et al. 1988) indicating that heavy ions have not thermalized. These studies were based on data accumulated over times much longer than the SW variations, and the results very likely have been affected by spatial and temporal averaging.

This article discusses recent observations of how the SW interacts with the bow shock using 3D distributions of H^+ and He^{++} ions measured by Cluster on a spin time resolution of 4 s. Comparisons of the velocity distributions in the upstream SW and downstream MS have shown that the SW can sometimes cross the bow shock with little or no heating. These observations show the SW ions can be transported across the shock in ways not predicted by any bow shock theory or models, and are important for understanding the physics of collisionless shock.

2. INSTRUMENTATION

Data from an electrostatic analyzer (ESA) experiment on Cluster specifically designed to measure the cold SW beam (g-detector) have been used. The detector includes eight sensors aligned along the polar (θ) direction separated by $\sim 5^\circ.625$, and the SW is detected in the eight ϕ -sectors ($5^\circ.625$) in the $\sim 45^\circ$ azimuthal ϕ -wedge aligned along the Sun–Earth line (Rème et al. 2001). This instrument is microprocessor-controlled and the high voltage (HV) sweeps only near the peak of the SW distribution and data from each of the 64 $\theta\phi$ directions can be examined separately. This capability allows us to identify the presence of the reflecting, gyrating, and leakage MS particles that permeate the vicinity of the bow shock and that contaminate the SW measurements (Montgomery et al. 1970; Thomsen et al. 1983; Scokpe 1995; Parks et al. 2012). Although these particles represent a small fraction of the SW (up to 20%), they have energies that are higher than the SW and affect the values of the bulk parameters calculated from the moments of the measured distribution. Another instrument (G-detector) with 16 sensors in the polar direction (θ) separated by $11^\circ.25$, measures the rest of the plasma. The two instruments, combined with the spin of the spacecraft, measure the full three-dimensional (3D) distribution in 4 s.

3. DATA SELECTION

“Solar wind” is a generic term referring to all particles escaping the Sun. The SW can be slow, fast, and turbulent, associated with different sources on the Sun, coronal holes, ICMEs and CIRs, for example. The observed SW thus come from different regions on the Sun whose composition, velocity, and temperatures of SW He^{++} and H^+ can be very different. To avoid mixing the measurements from the different source regions, we have studied the interaction of the SW with the bow shock for different SW velocities. The example we show below comes from the SW whose bulk speed was $\sim 400 \text{ km s}^{-1}$.

4. OBSERVATIONS

To illustrate that the SW beams can be detected in the downstream MS possessing nearly the same features of the upstream SW, we discuss the bow shock crossing that occurred on 2001 January 24. Cluster 3 was outbound and crossed the bow shock at ~ 0645 UT (Figure 1). The intense red line at $\sim 0.9 \text{ keV}$ in the energy flux spectrogram after 0645 UT is due to SW H^+ ions and the fainter green line above it at $\sim 1.8 \text{ keV}$ is due to He^{++} ions (from g-detector). The bulk parameters shown are computed on board from the measured spin-resolution 3D distribution functions of the g-detector, adding up all of the particles measured by the eight detectors in the $45^\circ \phi\theta$ wedge during one spin of the spacecraft. During this crossing, the instrument was operating in a mode that transmitted the spin-resolution SW distribution function once every 15 spins (60 s) and the remaining 14 spin data were not transmitted. Although the contributions of the reflected, gyrating, and leakage particles are minimized, note that some of the counts (blue) included contamination from these particles because there was overlap in energy (top panel).

Moments calculation show that the density of the SW on this day was $\sim 6.2\text{--}8.2 \text{ cc}^{-1}$ (panel 2 from the top, black) and the temperature was $\sim 1.15 \times 10^5 \text{ K}$ (10.1 eV) (panel 2, red). The mean SW velocities were $V_x = -408 \text{ km s}^{-1}$, and V_y and $V_z \sim -8 \text{ km s}^{-1}$ (third panel). The data in the next three panels come from the G-detector. This detector does not count in the SW and the bulk parameters after ~ 0645 UT are meaningless. The bottom panel shows that the magnitude of the magnetic field in the SW jumped from 4 nT to nearly 20 nT at the shock. Note that there was a considerable amount of low frequency magnetic variations in the MS. Timing from the four Cluster spacecraft showed that the bow shock was moving toward Earth with a speed of $\sim 12 \text{ km s}^{-1}$ and the thickness of the shock boundary was $\sim 20 \text{ km}$, slightly larger than the Larmor radius of 1 keV electrons in 20 nT B -field ($\sim 12 \text{ km}$). The Alfvén speed in the SW was $\sim 46 \text{ km s}^{-1}$, yielding an Alfvén Mach number $M_A \sim 8.9$. The plasma β of the SW was ~ 1.4 and the angle between the shock normal and the IMF was $\theta_{BN} \sim 62^\circ$. This bow shock was a typical supercritical quasi-perpendicular shock.

5. OBSERVATIONS IN THE MAGNETOSHEATH

The mean velocity of the plasma in the MS was $\sim 263 \text{ km s}^{-1}$. The Alfvén speed in the magnetosheath was $\sim 60 \text{ km s}^{-1}$ and the bulk velocity remained super-Alfvénic ($M_A \sim 4.4$). A PIC simulation model has predicted that bulk flows in

the MS can remain super-Alfvénic in regions away from the Sun–Earth line (Yang et al. 2016). Slightly different values were detected on SC 1 separated by a few hundred kilometers, indicating that the SW was not spatially uniform over distances of an ion gyro-radius. The plasma in the downstream region was nearly isotropic and the temperature estimated from the distribution function obtained yielded $\sim 103\text{--}296 \text{ eV}$ ($1.18\text{--}3.37 \times 10^6 \text{ K}$), but they included other MS particles. The downstream β measured varied from ~ 3 to 10.

6. SW DISTRIBUTIONS IN THE MAGNETOSHEATH

The SW beams can directly penetrate across the bow shock and can persist in the MS for a long time before they are thermalized (Sckopke 1995). The distribution functions of the penetrated SW beams into the MS have been computed from the g-detector from 0632:04 UT to 0646:07 UT in the SW (Figure 2). Here $v = (v_x^2 + v_y^2 + v_z^2)^{1/2}$. The moments of the bulk parameters shown in Figure 1 come from these distributions. The density in the MS varied from ~ 1.7 to 9.7 cc^{-1} , bulk velocity varied from 247 to 396 km s^{-1} , and temperature varied from ~ 13 to 132 eV . Note that the distributions are very complex, sometimes showing multiple beams. A few events showed broadening of the H^+ and He^{++} peaks, indicating that the beams have been heated (0637:06), while others (0632:06 UT; 0638:07, 0638:07) showed the H^+ and He^{++} beams remaining almost the same, as in the upstream SW (0646:07). Note that the He^{++} ions did not slow down as much as the H^+ ions (0632:06 UT).

7. TEMPERATURE DETERMINATION

The temperatures of the SW and MS beams can be estimated much more accurately using the detailed measurements of the distribution function after removing the contributions of the reflected, gyrating, and escaping MS particles. We use the $\phi\theta$ distributions to locate the contaminations and separate them from the actual SW beams. The top two rows of Figure 3 (0645:07 UT) and the bottom two rows (0632:07 UT) show (two-dimensional) 2D distributions of the SW in the upstream and downstream regions in the plasma frame. To compute temperatures of H^+ and He^{++} in the SW, the velocities have been shifted by -411 km s^{-1} and -575 km s^{-1} , respectively. The corresponding velocity shifts in the MS are -297 and -501 km s^{-1} . The ratio of the bulk velocity of He^{++} to H^+ in the SW is ~ 1.4 . The ratio of the bulk speeds for He^{++} to H^+ in the MS is ~ 1.7 because the He^{++} with greater M/Q slows down less than H^+ .

These distributions have been subsequently transformed to directions parallel (x -axis) and perpendicular (y -axis) to the magnetic field and the 1D cuts were then taken to obtain parallel (red) and perpendicular (black) temperatures, assuming the shapes of the distributions are Maxwellian. Two constraints are required for fitting. One is to put drift velocity = 0, which shifts the fitting curves to be located at the center ($v = 0$). The other is to colocate the peaks of $f(v_{\parallel})$ and $f(v_{\perp})$. Also, the centers of the distributions are located at the center as closely as possible. If $f(v_{\parallel})$ or $f(v_{\perp})$ do not go through the center, the temperature will be estimated as being slightly smaller. The computed SW temperatures (in eV) of the beams in the parallel

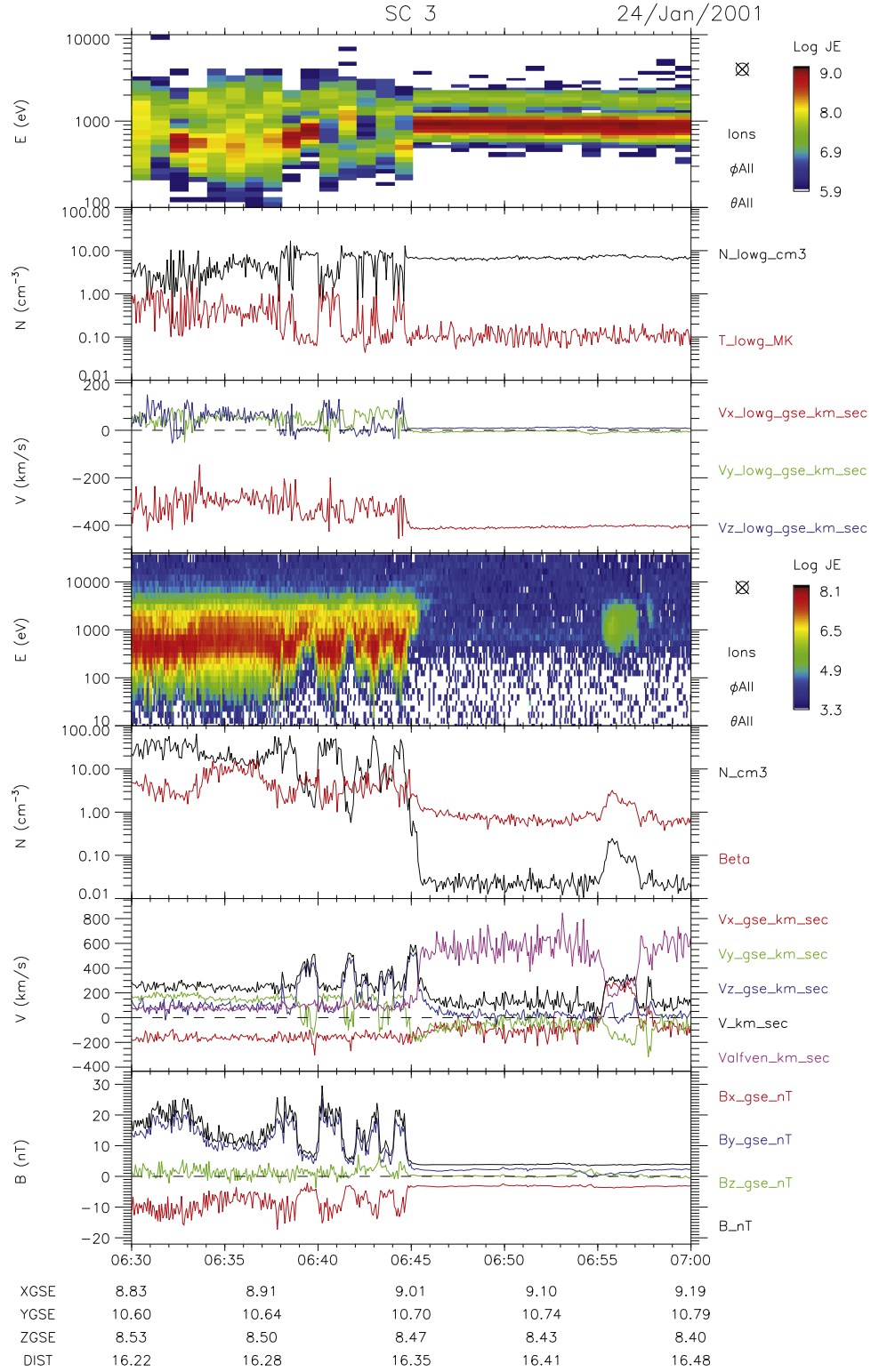


Figure 1. The top panel shows the energy flux spectrogram from the SW g-detector, which has eight sensors along the polar direction separated by $\sim 5^\circ$ and counts particles as the spacecraft spins in the $\sim 45^\circ$ ϕ -wedge aligned along the Sun–Earth direction. The next two panels are density (black) and temperature (red) and mean velocities computed from the velocity moments. Note that the mean flow in the MS remains super-Alfvénic (panel 5 from the top, Alfvén speed, magenta). The bottom panel shows the spin-averaged magnetic field data (4 s). All quantities are shown in GSE coordinates.

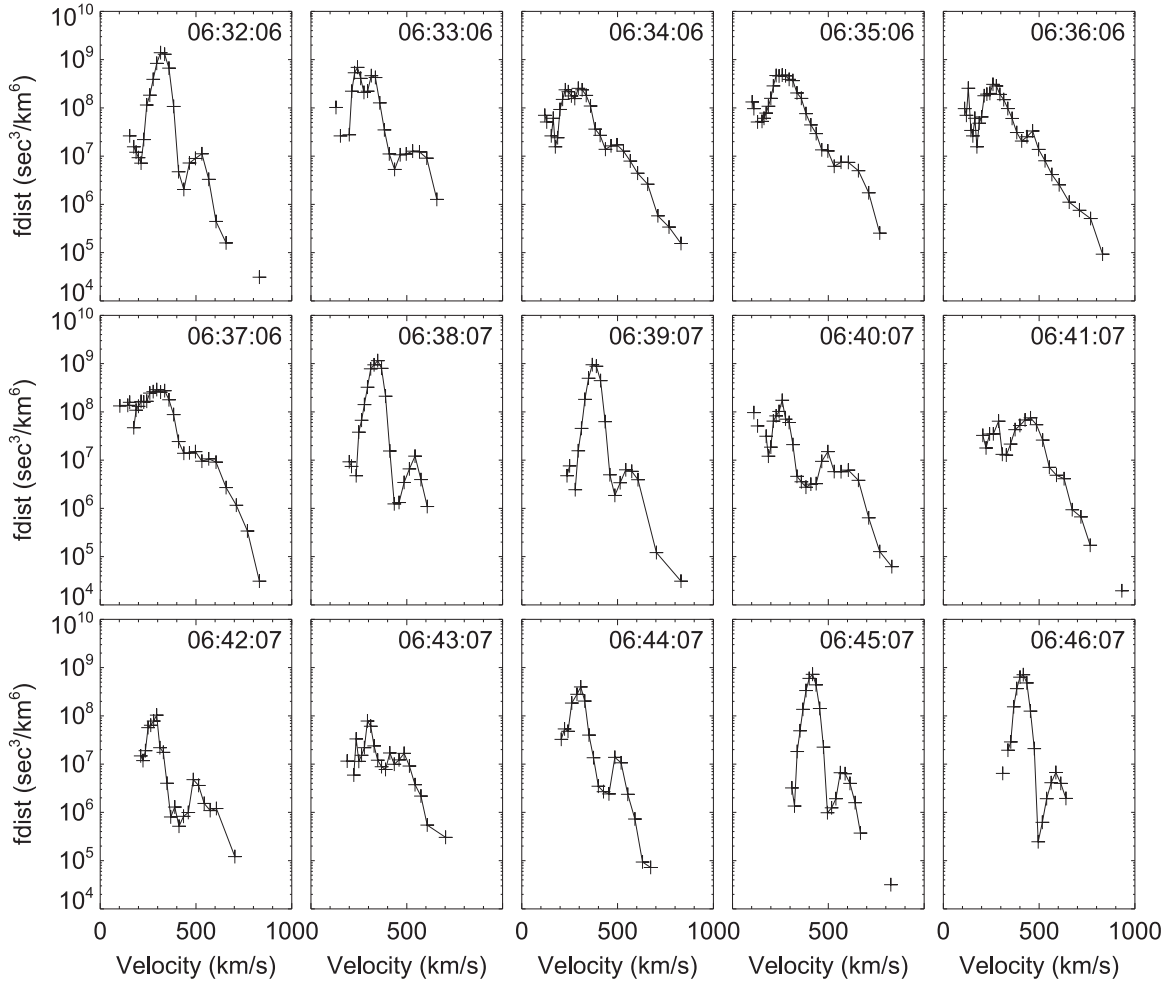


Figure 2. Spin-resolution 3D distribution function of ions detected on Cluster 3 from 0632:04 in the MS to 0646:07 in the SW in the spacecraft frame of reference. Cluster was in a mode that transmitted the distribution function about every minute. The vertical axis is the distribution function calculated by summing all of the counts from the different θ detectors (θ goes from $+90^\circ$ to -90° with $+90^\circ$ along the spacecraft spin axis) in the 45° ϕ wedge in the azimuthal direction. The main beam is H^+ and the weaker beam is He^{++} . The quality of the SW beams in the MS varied considerably, with some showing features of H^+ and He^{++} that were nearly the same as in the SW (0632:06 UT), while others have been scattered and heated. The foot of the shock was crossed at $\sim 0645:07$ UT and the distribution at 0644:07 was near the peak of the ramp.

and perpendicular directions for H^+ and He^{++} in the SW and MS are shown below.

			T_{\parallel}	T_{\perp}		T_{\parallel}	T_{\perp}
Solar wind	0646:07 UT	H^+	9.62	7.54	He^{++}	8.35	5.2
Magnetosheath	0632:07 UT	H^+	6.09	5.78	He^{++}	7.33	14.4
	0638:07 UT	H^+	6.29	6.31	He^{++}	5.65	7.98
	0639:07 UT	H^+	10.4	7.71	He^{++}	13.3	7.52

These observations generally show $T_{\parallel} > T$ for both H^+ and He^{++} , and T_{\parallel} and T_{\perp} are slightly lower in the MS than in the SW, except for 0639:07 UT. Also, for He^{++} in the MS, T_{\perp} is higher than T_{\parallel} .

The temperature anisotropy in the SW is consistent with measurements from *WIND* (Kasper et al. 2003; Liu et al. 2006) and *Helios* that indicate T_{\parallel} is often higher than T_{\perp} . The surprising result is that the temperatures of H^+ and He^{++} can be nearly the same in the downstream MS region as in the SW and confirms the early *Helios* results (Formisano et al. 1970). Note that the temperatures estimated here for the beams are almost a factor of two lower than those shown in Figure 1 that included the other particles (~ 10 – 12 eV).

8. ELECTROSTATIC POTENTIAL ACROSS EARTH'S BOW SHOCK

A feature regularly observed when the SW crosses the shock is the deceleration of the SW indicated by the shifting of the SW beam energy to lower values in the MS. Shock models attribute such SW ion slowdown to electric potential set up by the finite Larmor radius effect of ions and electrons, in which the ions penetrate further inside the boundary than the electrons (Feldman 1985). If we assume the ion slowdown of 100 km s^{-1} is entirely due to the potential $\Delta\phi$ between the upstream and downstream, use of the relation $mV_{sw}^2/2 - mV_{MS}^2/2 = q\Delta\phi$ yields $\Delta\phi \sim 50$ Volts.

The 1D electron distribution in the SW is nearly isotropic but that in the MS has a higher temperature and a flat top shape (Figure 4). The edge of the flat top is ~ 4 – $6 \times 10^3 \text{ km s}^{-1}$ for electrons coming from the SW side and $(4$ – $7) \times 10^3 \text{ km s}^{-1}$ for electrons coming from the Earthward side. Taking the edge of the flat top velocities as being due to the lower energy electrons not being able to overcome the electric potential, originally proposed by Feldman (1985), the potential drop we obtain is essentially the same value as the potential deduced from the ions. Our estimates of ~ 50 Volts for the potential drop are

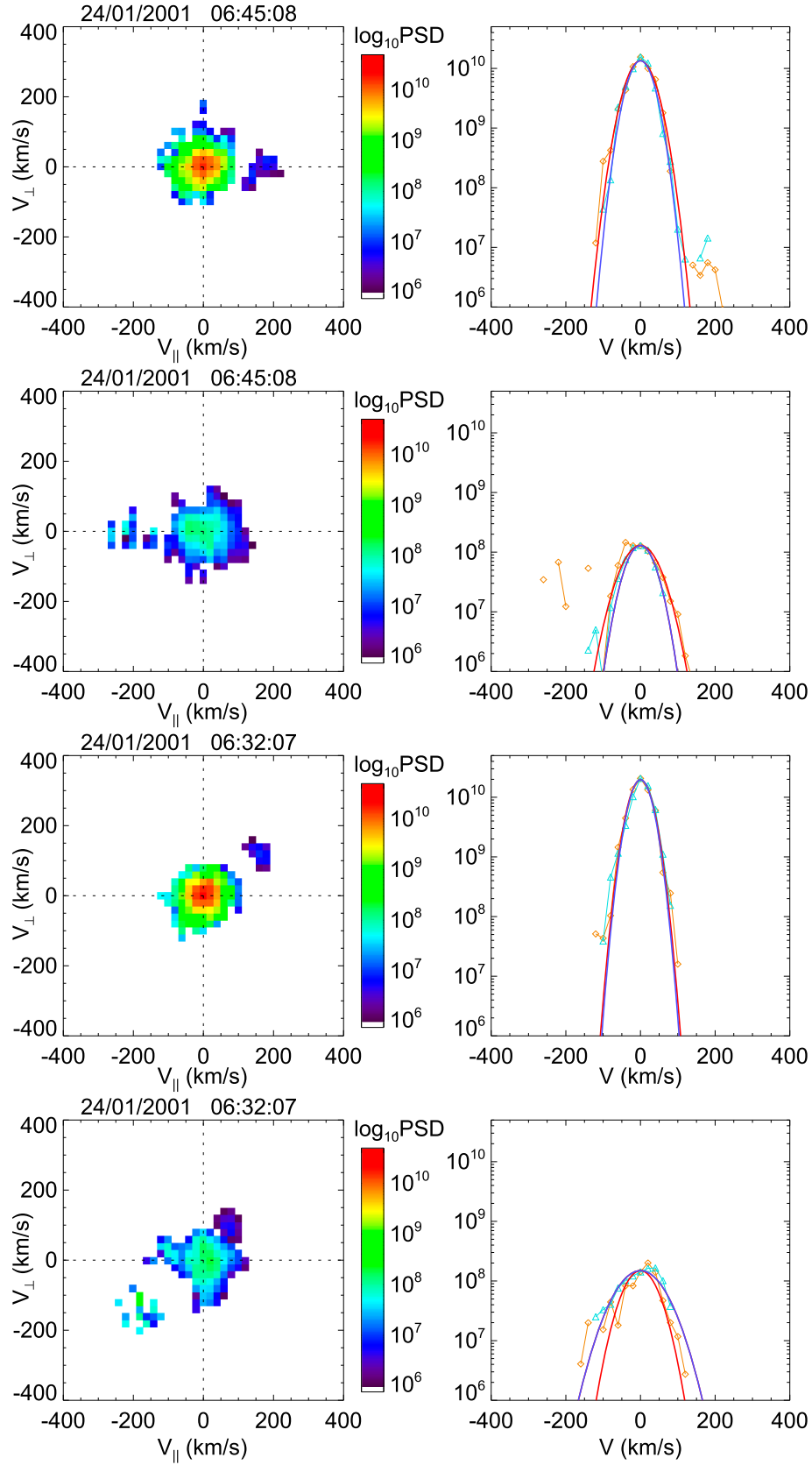


Figure 3. Estimates of the temperature of H^+ and He^{++} beams in the plasma frame of reference. The top four panels show the 2D and one-dimensional (1D) cuts of the beams in the SW (0645:06 UT) and the bottom panels (0632:06 UT) show those in the MS. In the 1D distributions, the data points are circles and the solid lines are Maxwellian fits. Red is T_{\parallel} and blue is T_{\perp} . The SW beam crossing the bow shock is deviated and slowed down but clearly discernible. Velocity scales are $\pm 400 \text{ km s}^{-1}$. The color bar gives the phase space density in units of $\text{s}^3 \text{ m}^{-6}$.

lower than the few hundred Volts reported previously by Formisano (1982) and Wygant et al. (1987). Note that the SW beam energy in the MS is highly varying, indicating that the potential drop across the bow shock is not uniform.

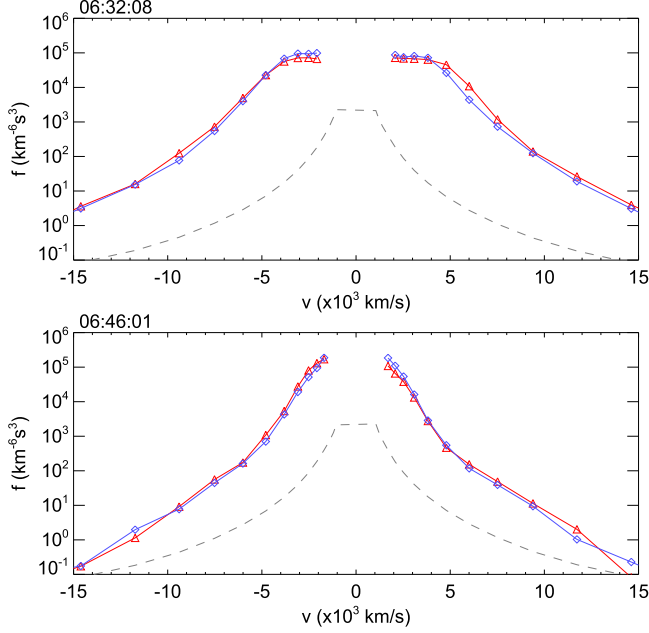


Figure 4. Examples of the parallel (red) and perpendicular (blue) electron distribution functions in the MS (top, 0632:08) and in the SW (bottom, 0646:01). The dashed curve represents a one-count level. The missing data at $V \sim 0$ km s⁻¹ are photoelectrons that have been removed.

9. STATISTICAL RESULTS

To determine where the SW beams penetrate into the MS across the bow shock, we have examined 111 bow shock crossings that occurred during 2001 and 2002. Our observations come from both quasi-perpendicular and quasi-parallel shock regions (Figure 5). A preliminary determination of the direction of the shock normal n was made using minimum variance analysis (MVA) method. We calculated $\cos^{-1}(n \cdot B / |n \cdot B|)$ and divided the shocks into two groups. If the value is between 45° and 135°, the shock was designated a perpendicular shock; otherwise the shock was considered a parallel shock. Forty-seven crossings showed the SW H⁺ beams penetrating the MS. Of those 47 crossings, 30 were in the perpendicular shock region and 17 were in the parallel shock region (Figure 5).

For the 111 crossings, the density of H⁺ ions varied from 3 to 18 cc⁻¹. The SW bulk speed during 53 crossings was >500 km s⁻¹, 400–500 km s⁻¹ for 30 crossings, and 300–400 km s⁻¹ for 22 crossings. The parallel temperatures of H⁺ ions in the SW in all of the 47 events studied were higher than the perpendicular temperatures, with typical $T_{\parallel}/T_{\perp} \sim 1.5$ –3. The beams in 13 crossings were good, retaining many of the upstream SW features, 22 were moderate and 12 were poor but still discernible. Generally, more good beams were observed in the quasi-perpendicular shock region when the SW temperature was lower (not shown). The other 64 crossings showed that thermalization of varying degrees had occurred crossing the shock. The SW Alfvén Mach number for the 111 events varied from ~3–12 and the 47 crossings with MS beams varied from 3 to 10.

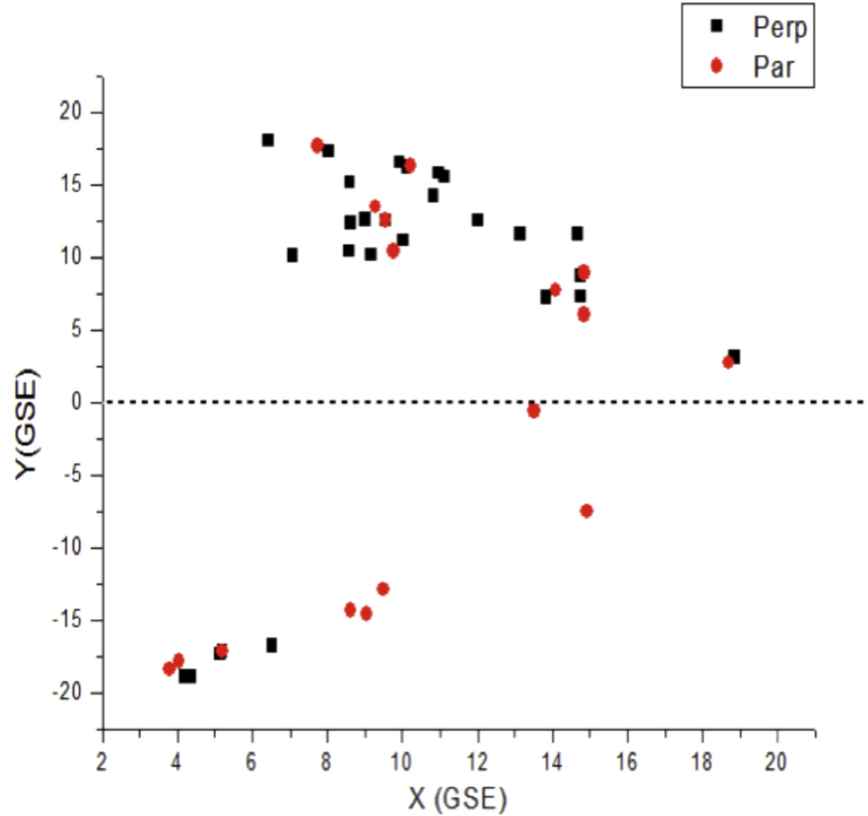


Figure 5. Locations of 41 cases from a sample of 111 crossings observed by Cluster in 2001–2002 where the SW beams have been clearly observed in the magnetosheath (GSE coordinates). SW beams are observed in the MS in both the quasi-perpendicular and quasi-parallel shock regions. X is positive toward the Sun and Y toward dusk. The black squares represent calculated $\theta_{BN} > 45^\circ$ and the red squares $< 45^\circ$.

10. SUMMARY AND DISCUSSION

The main focus of our study was to learn how the SW interacts with the bow shock containing minimal contribution from the reflected, gyrating and leakage MS particles. Our results show that the temperatures of the H^+ and He^{++} beams in the MS can be nearly the same as those found in the SW. The SW beams penetrating into the MS can be found in both quasi-parallel and quasi-perpendicular regions of the bow shock. We also showed that the slowing down of the SW crossing into the MS is consistent with the electrostatic potential across the shock (Scholer et al. 2003). However, none of the bow shock models predict that the SW can cross the bow shock with little or no heating.

The temperatures of H^+ and He^{++} of the SW for 2001 January 24 are representative of the 13 crossings that we have examined, but are different from those reported earlier by Robbins et al. (1970), who showed that the most probable temperature ratio of He^{++} to H^+ ions in the SW is four, corresponding to the same thermal speed. However, the SW data used by Robbins et al. (1970) did not distinguish between slow and fast streams and included the times of coronal holes, CIRs, and ICMEs. As mentioned above, plasmas originating from different solar regions have different dynamics, producing different temperatures for H^+ and He^{++} ions. A cursory survey of Cluster data for temperature ratios in fast SW streams associated with several ICMEs and CIRs indicates that they can vary from ~ 3 to 15 (not shown).

Determining the SW temperature accurately is fundamentally important for understanding the dynamical processes responsible for the SW generation. There are many theories about the thermal state of the SW H^+ component (Parker 1965; Sturrock & Hartle 1966; Burlaga & Ogilvie 1970; Eviater & Schulz 1970; Forslund 1970; Hollweg 1971; Wolffe et al. 1971; Chen et al. 1972; Whang 1972; Barnes & Hung 1973; Hundhausen 1973; Feldman et al. 1974) and these theories require accurate measurements of the temperatures.

We do not know if the temperature of the SW measured at 1 au is the temperature at the source on the Sun, but our observations of nearly the same temperature indicate that the two ion species are in equilibrium. Equipartition of energy between the H^+ and He^{++} ions can be achieved by Coulomb collision. Feldman et al. (1974) studied possible timescales to transfer energy by collision against expansion times of the SW and concluded that a suitable condition could exist on the Sun to produce the ratio 1. However, since our observations are made at 1 au, it is not possible to discount that our SW observations could have undergone wave-particle interaction in transit, reducing the pitch-angle anisotropy (Hellinger et al. 1996; Marsch et al. 2006).

We have begun comparing our 111 observations with electrons and electromagnetic waves across the shock and also with PIC simulations. Preliminary results from a 1D PIC

simulation model show that SW beams can be observed in the MS when the spacecraft is close to the boundary. However, the beams generally are not observed very far into the MS. Our plan is to improve the 1D PIC simulation to a 2D PIC model (Yang et al. 2016), using our observations as input. The results will be presented in future publications.

The research at UC Berkeley was performed under NASA Grant No. NNX07AP96G. Cluster is a joint project of the ESA and NASA. The research work by E. Lee was supported in part by the BK21 Plus Program and the Basic Science Research Program (NRF-2013R1A1A2010711) through the National Research Foundation funded by the Ministry of Education of Korea.

REFERENCES

- Auer, P. L., Kilb, R. W., & Crevier, W. F. 1971, *JGR*, **76**, 2927
 Barnes, A., & Hung, R. J. 1973, *CosEl*, **3**, 416
 Burlaga, L., & Ogilvie, K. 1970, *ApJ*, **159**, 659
 Chapman, S., Lee, R. E., & Dendy, R. O. 2005, *SSRv*, **121**, 5
 Chen, W., Lai, S., Liu, H., & Lin, W. 1972, *JGR*, **77**, 1
 Ellacot, S. W., & Wilkinson, W. P. 2003, *JGR*, **108**, 1409
 Eviater, A., & Schulz, M. 1970, *P&SS*, **18**, 321
 Feldman, W. C. 1985, in *Collisionless Shocks in Heliosphere: Reviews of Current Research*, Vol. 35, ed. B. T. Tsurutani, & R. G. Stone (Washington, DC: American Geophysical Union), 195
 Feldman, W. C., Asbridge, J. R., & Bame, S. J. 1974, *JGR*, **79**, 2319
 Formisano, V. 1982, *GeoRL*, **9**, 1033
 Formisano, V., Palmiotto, F., & Moreno, G. 1970, *SoPh*, **15**, 479
 Forslund, D. W. 1970, *JGR*, **75**, 17
 Fuselier, S. A., Shelley, E. G., & Klumper, D. M. 1988, *GeoRL*, **15**, 1333
 Gedalin, M. 1997, *SGeo*, **18**, 541
 Hellinger, P., Mangeney, A., & Matthews, A. 1996, *GeoRL*, **23**, 621
 Hollweg, J. V. 1971, *JGR*, **76**, 7491
 Hundhausen, A. J. 1973, *JGR*, **78**, 1528
 Kasper, J. C., Lazarus, A. J., Gary, S. P., & Szabo, A. 2003, in *Solar Wind 10: Proc. Tenth Int. Solar Wind Conf.*, ed. M. Velli, R. Bruno, & F. Malara (Melville, NY: AIP), 538
 Kennel, C. F., Edmiston, J. P., & Hada, T. 1985, in *Collisionless Shocks in the Heliosphere: A Tutorial Review*, Vol. 34, ed. R. G. Stone, & B. T. Tsurutani (Washington, DC: American Geophysical Union), 1
 Krall, N. A. 1997, *AdSpR*, **20**, 715
 Liu, Y., Richardson, J. D., Belcher, J. W., et al. 2006, *JGR*, **111**, A01102
 Marsch, E., Zhao, L., & Tu, C.-Y. 2006, *AnGeo*, **24**, 2057
 Montgomery, M. D., Asbridge, J. R., & Bame, S. J. 1970, *JGR*, **75**, 1217
 Parker, E. N. 1965, *SSRv*, **4**, 666
 Parks, G. K., Lee, E., McCarthy, M., et al. 2012, *PhRvL*, **108**, 061102
 Peterson, W. K., Shelley, E. G., Sharp, R. D., et al. 1979, *GeoRL*, **6**, 667
 Rème, H., Aoustin, C., Bosqued, J. M., et al. 2001, *AnGeo*, **19**, 1303
 Robbins, D. E., Hundhausen, A. J., & Bame, S. J. 1970, *JGR*, **75**, 1178
 Scholer, M., Shinohara, I., & Matsukiyo, S. 2003, *JGR*, **108**, 1014
 Skopke, N. 1995, *AdSpR*, **15**, 261
 Sturrock, P. A., & Hartle, R. E. 1966, *PhRvL*, **16**, 628
 Thomsen, M. F., Gosling, T., Bame, S. J., et al. 1983, *GeoRL*, **10**, 1207
 Whang, Y. C. 1972, *ApJ*, **178**, 221
 Wolffe, C. L., Brandt, J. C., & Southwick, R. G. 1971, *ApJ*, **165**, 181
 Wu, C. S., Winske, D., Zhou, Y. M., et al. 1984, *SSRv*, **37**, 63
 Wygant, J. R., Bensadoun, M., & Mozer, F. S. 1987, *JGR*, **92**, 11109
 Yang, Z., Huang, C., Liu, Y. D., et al. 2016, *ApJ*, in press